Routledge
Taylor & Francis Group

Check for updates

Human hippocampal theta oscillations reflect sequential dependencies during spatial planning

Raphael Kaplan [ID][a,b], Adrià Tauste Campo[c,d,e], Daniel Bush[f,g], John King[f,h], Alessandro Principe[d], Raphael Koster[a,f], Miguel Ley Nacher[d], Rodrigo Rocamora[d] and Karl J. Friston [ID][a]

[a]Wellcome Centre for Human Neuroimaging, UCL Institute of Neurology, University College London, London, UK; [b]Kavli Institute for Systems Neuroscience, Norwegian University of Science and Technology, Trondheim, Norway; [c]Center for Brain and Cognition, Department of Information and Communication Technologies, Universitat Pompeu Fabra, Barcelona, Spain; [d]Epilepsy Unit, Department of Neurology, Hospital del Mar Medical Research Institute (IMIM), Barcelona, Spain; [e]Barcelonaβeta Brain Research Center, Pasqual Maragall Foundation, Barcelona, Spain; [f]UCL Institute of Cognitive Neuroscience, University College London, London, UK; [g]UCL Queen Square Institute of Neurology, University College London, London, UK; [h]Clinical, Education and Health Psychology, University College London, London, UK

ABSTRACT

Movement-related theta oscillations in rodent hippocampus coordinate 'forward sweeps' of location-specific neural activity that could be used to evaluate spatial trajectories online. This raises the possibility that increases in human hippocampal theta power accompany the evaluation of upcoming spatial choices. To test this hypothesis, we measured neural oscillations during a spatial planning task that closely resembles a perceptual decision-making paradigm. In this task, participants searched visually for the shortest path between a start and goal location in novel mazes that contained multiple choice points, and were subsequently asked to make a spatial decision at one of those choice points. We observed ~4–8 Hz hippocampal/medial temporal lobe theta power increases specific to sequential planning that were negatively correlated with subsequent decision speed, where decision speed was inversely correlated with choice accuracy. These results implicate the hippocampal theta rhythm in decision tree search during planning in novel environments.

Introduction

Recent evidence has linked the hippocampus with planning in rodents (Miller, Botvinick, & Brody, 2017) and humans (Kaplan et al., 2017a). Moreover, changes in hippocampal theta power (approx. 4–8Hz in humans) have been observed during memory-guided decision-making in well-learned environments in both species (Belchior, Lopes-Dos-Santos, Tort, & Ribeiro, 2014; Guitart-Masip et al., 2013; Schmidt et al., 2013). However, it remains unclear whether changes in hippocampal theta power are associated with planning in novel environments. Notably, rodent type I hippocampal theta oscillations generated by exploratory movement (Vanderwolf, 1969) are linked to sweeps of place cell activity produced by hippocampal theta phase precession (O'Keefe & Recce, 1993). It has been hypothesized that these 'theta sweeps' could serve as a mechanism to plan trajectories online (Johnson & Redish, 2007). This raises the possibility that similar increases in human hippocampal theta power are induced by the planning of forward trajectories.

To investigate the role of the hippocampal theta rhythm in online spatial planning (i.e., the search of decision trees), we created a spatial task that required little to no learning, in which participants could draw upon their experience in the physical world (Kaplan et al., 2017a). We tested human participants on this task using noninvasive whole-head magnetoencephalography (MEG). Participants were instructed to visually search for the shortest path between a start and goal in novel mazes that afforded multiple paths. Participants were then asked which direction they would take from one of two choice points along the shortest path (Figure 1).

Crucially, the mazes were designed to induce forward planning in terms of a two-level tree search, where participants needed to maintain the decisions they made at each choice point. At both choice points, there was a small, medium, or large path length difference – creating a total of (3x3) nine conditions allowing us to test the effect of planning demands at each choice point depth (i.e., initial or second). In parallel, our task also contained a non-sequential control condition, where participants were presented with mazes containing only one choice point (Figure 1(d)). In either case, we associate a smaller path
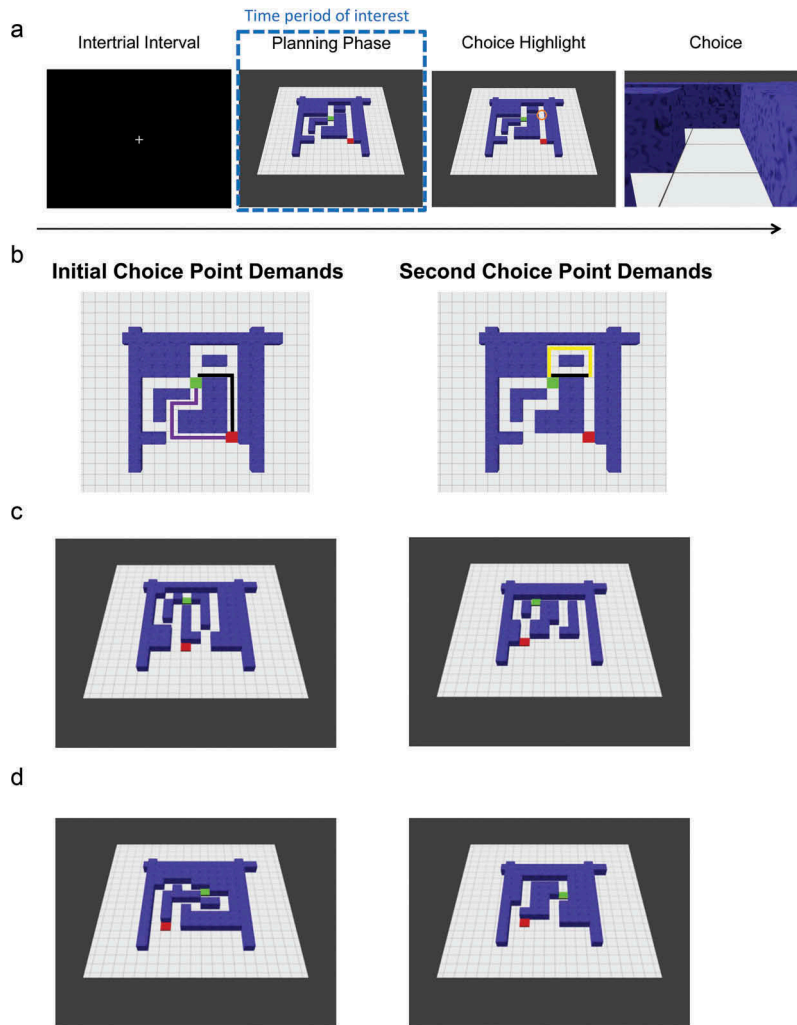
Figure 1. Task. A. Each trial (i.e., visually presented maze) began with an inter-trial interval (ITI) of 1.5s. Next, during a 3.25s planning phase, participants had to infer the shortest path from a start point (red square) to a goal location (green square) and remember the chosen direction for each choice point along the shortest path. A choice point was subsequently highlighted (choice highlight) for 250ms. This was either the initial (i.e. first) or second (i.e. subsequent) choice point along the shortest path. Participants were then asked which direction (e.g., left or forward) they would take at that choice point during a choice period that was cued by a first-person viewpoint of the highlighted location. Participants had a maximum of 1.5s to make their choice using a button box. B. Overhead view (not shown during the experiment) of the maze in A, indicating which path lengths contribute to initial and second choice point demands (black line represents shortest path). C. Left: Example sequential planning trial with a small path length difference (demanding) at the red square/initial choice point and large (less demanding) path length difference at the second choice point. Right: Example trial with a large (less demanding) path length difference at the red square/initial choice point and small (demanding) path length difference at the second choice point. D. Left: Example non-sequential (control) trial with a small path length difference (demanding). Right: Example non-sequential (control) trial with a large path length difference (less demanding).

difference with greater ambiguity and processing demands. Importantly, in any trial, participants were only prompted to make one choice after seeing the full maze; however, until the choice point was highlighted, they did not know which decision would be probed in sequential planning trials (Figure 1). After planning their route, participants were asked to choose – at a specified choice point – the direction of the shortest path to the goal location (Figure 1). This provided a measure (reaction time, RT) with which to quantify their (subjective) uncertainty to complement the (objective) difference in path lengths.

This design allowed us to ask whether hippocampal theta power relates to successful sequential spatial planning.

Methods

Participants

MEG
Twenty-four participants (14 female: mean age 23.5 yrs; SD of 3.49 years) gave written consent and were compensated for performing the experimental task, as

approved by the local research ethics committee at University College London in accordance with Declaration of Helsinki protocols. All participants had normal or corrected-to-normal vision and reported to be in good health with no prior history of neurological disease. Due to technical difficulties, two participants were removed from our sample, leaving twenty-two participants in the behavioral and MEG analyses presented here.

iEEG

Pre-surgical EEG recordings from 2 patients with pharmacoresistant focal-onset seizures and hippocampal depth electrodes gave written consent, as approved by the local ethics committee at Hospital del Mar and in accordance with Declaration of Helsinki protocols. One patient was removed from analyses, because of visual difficulties due to an inferior occipital lesion, leaving one patient with normal vision presented in the current analysis. A summary of the patient's characteristics is given in Table 1.

Experimental design

During MEG scanning, stimuli were presented via a digital LCD projector on a screen (height, 32 cm; width, 42 cm; distance from participant, ~70 cm) inside a magnetically shielded room using the Cogent (http://www.vislab.ucl.ac.uk/cogent.php) toolbox running in MATLAB (Mathworks, Natick, MA, USA). Instead of a projector, the iEEG patient completed the task on a laptop in their hospital bed. There were no other differences with the MEG experiment unless mentioned otherwise. Over the course of 220 trials, participants viewed 220 different mazes from a slightly tilted (overhead) viewpoint and later chose from first-person viewpoints within mazes generated using Blender (http://www.blender.org). All mazes had a starting location (a red square) toward the bottom of the maze and a goal location (a green square) further into the maze (Kaplan et al., 2017a). Mazes differed by hierarchical depth (number of paths to a goal location): there were 110 mazes with four possible routes (sequential mazes) and a further 110 non-sequential control mazes with two possible routes (control mazes). In the

scanner, participants were first presented with pictures of novel mazes (Figure 1) of varying difficulty (from an overhead viewpoint) and then asked to determine the shortest path from a starting location (a red square) at the bottom of the screen to the goal location (a green square). The overhead view appeared on the screen for 3.25 s, after which a location (choice point) along the path was highlighted briefly for 250 ms with an orange circle. The choice point location could either be the initial choice point or a second (subsequent) choice point. Crucially, participants would only have to make a decision about one choice point for each trial.

At either choice point, it was necessary to choose between two possible directions, which could be left, forward, or right, with an additional option to select equal, if both routes were the same distance. The second choice point always fell on the optimal path from the starting location to the goal(Kaplan et al., 2017a). After the choice point was highlighted, a 'zoomed in' viewpoint of this location (always one square back and facing the same direction as the overhead viewpoint) was presented. Participants had less than 1.5s (2s for the iEEG patient) to decide whether to go left, forward, right, or decide that all directions were equidistant to the goal. If no button press was made within the allotted duration, the trial counted as an incorrect trial and the experiment moved on to the 1.5s inter-trial interval (ITI) phase. Participants repeated this trial sequence 110 times per session, for a total of two sessions. Sessions lasted approximately 10–15 min.

All participants completed a brief practice session consisting of 40 mazes/trials before the experiment (on a laptop outside of the scanner). Sequential mazes contained two branch/choice points between routes further in the maze, and the path lengths from the initial choice point to either of the second choice points were always equal. In sequential mazes, we used a 3 × 3 factorial design. Path length differences were split between 2 (small difference), 4 (medium difference), or 6 (large difference) squares (for an example, see square tiles in the mazes presented in Figure 1) for the two paths at the starting location and a path length difference of 2, 4, or 6 squares at the optimal choice point in the maze. There was one catch trial for sequential and control mazes in

Table 1. Patient information.

Age/ Sex	Handedness	Seizure Onset/Freq	Education	Epileptic Focus	Drugs & Dosage	First-language
23M	R (but used L due to IV)	16 yo (1 seizure per week and now seizure free)	Secondary	R Temporobasal (temporal pole)	Eslicarbazepinole 1000 mg/per day; leviteracetam 1500/2x day; Perampanel 8 mg/per day	Spanish

All diagnostic and surgical procedures were approved by the clinical ethics committee of Hospital del Mar in accordance with the principles expressed by the Declaration of Helsinki. Electrode locations were determined solely by clinical criteria, ascertained by visual inspection of post-implantation MRI scans using Slicer 4 (Fedorov et al., 2012; www.slicer.org) and verified by an fMRI expert (R.Ka.). The Patient was seizure free for at least 24 h before participation and underwent an extensive neuropsychological evaluation to check for any cognitive impairments.

each session, each containing all equal path lengths (path length differences of 0). In sum, sequential maze trials could be 2, 2; 2, 4; 2, 6; 4, 2; 4, 4; 4, 6; 6, 2; 6, 4; 6, 6; (e.g. 4, 2 would have a medium path length difference of 4 at the starting location, whereas the second choice point would have a small path length difference of 2). Half of the trials in the experiment were control/non-sequential mazes, which only contained one choice point at the red starting square. For these mazes, path length differences were split between 2, 4, and 6, with one catch trial per session having equal path lengths.

iEEG recordings and artifact detection

All iEEG recordings were performed using a standard clinical EEG system (XLTEK, subsidiary of Natus Medical, Pleasanton, CA) with a 500 Hz sampling rate. A unilateral implantation in the right hemisphere was performed accordingly, using 15 intracerebral electrodes (Dixi Médical, Besançon, France; diameter: 0.8 mm; 5 to 15 contacts, 2 mm long, 1.5 mm apart) that were stereotactically inserted using robotic guidance (ROSA, Medtech Surgical, New York, NY).

Intracranial EEG signals were processed in a monopolar referencing montage because it has been found to be more sensitive than other montages in capturing hippocampal electrophysiological signals (Vila-Vidal et al., 2019). Still, it is important to note that monopolar referencing yields data that can be contaminated by volume conduction and remote field effects. All recordings were subjected to a zero phase, 400th order finite impulse response (FIR) band-pass filter to focus on our frequency range of interest (0.5–48 Hz) and remove the effect of alternating current. Audio triggers produced by the stimulus presentation laptop were recorded on the monitoring system, which allowed for the EEG to be aligned with trial onset information sampled at 25 Hz.

Although the patient was consistently engaged by the task, all trials that included interictal spikes (IIS) or other artifacts, either within the period of interest or during the padding windows, were excluded from all analyses presented here after manual inspection (4 trials removed). A 500 ms padding window was used at either end of planning period time series to minimize edge effects in subsequent analyses.

iEEG time-frequency analysis

Estimates of dynamic oscillatory power during periods of interest were obtained by convolving the EEG signal with a Morlet wavelet and squaring the absolute value of the convolved signal. The wavelet transform was preferred to the Fourier transform here since the analysis was focused on preserving temporal information about when power changes happened, which is in contrast with MEG analyses that were more focused on source localization. To perform baseline correction on time–frequency data for display purposes, power values were averaged across ITI periods for each frequency band, and those average values were subtracted from the power values at each time point in the planning period. To assess correlations among oscillatory power in each trial with RT, oscillatory power at each time point and frequency of interest was correlated with trial-by-trial RTs. These values were then averaged across the deepest contacts in both anterior (x:34, y:-13, z:-23) and posterior (x:33, y:-31, z:-9) right hippocampal electrodes to provide a single value at each time and frequency point for the patient.

MEG recording and preprocessing

Data were recorded continuously from 274 axial gradiometers using a CTF Omega whole-head system at a sampling rate of 600 Hz in third-order gradient configuration. Participants were also fitted with four electroculogram (EOG) electrodes to measure vertical and horizontal eye movements. MEG data analyses made use of custom made Matlab scripts, SPM8 &12 (Wellcome Center for Human Neuroimaging, London; Litvak et al., 2011), and Fieldtrip (Oostenveld, Fries, Maris, & Schoffelen, 2011). For preprocessing, MEG data was epoched into 2s baseline periods prior to the planning phase for each of the nine sequential planning conditions of interest and the three non-sequential planning control conditions. Trials were visually inspected, with any trial featuring head movement or muscular artifacts being removed (mean trials removed per participant = 3.45).

MEG source reconstruction

The linearly constrained minimum variance (LCMV) scalar beamformer spatial filter algorithm was used to generate source activity maps in a 10-mm grid (Barnes & Hillebrand, 2003). Coregistration to MNI coordinates was based on nasion, left and right preauricular fiducial points. The forward model was derived from a single-shell model (Nolte, 2003) fit to the inner skull surface of the inverse normalized SPM template. The beamformer source reconstruction algorithm consists of two stages: first, based on the data covariance and lead field structure, weights are calculated which linearly map sensor data to each source location; and second, a summary statistic based on the mean oscillatory power between experimental conditions is calculated for each voxel. Focusing on the specifics of power estimation, sensor

data have a Hann window applied and are then subject to a Fast Fourier transform (FFT) to estimate power at each frequency across the whole signal. FFT data from each sensor is then multiplied by the beamformer weights to estimate power in each source.

We wished to control for any possible influence of EOG muscular artifacts during the planning period on estimates of oscillatory power and therefore computed the variance of two simultaneously recorded EOG signals across each planning phase and removed any covariance between these EOG variance values and oscillatory power measurements across voxels by linear regression (Kaplan et al., 2017c, 2014). This left 'residual' oscillatory power measurements for all trials whose variance could not be accounted for by changes in the EOG signal between trials, and these residual values were used as summary images for subsequent analyses. RT was included as an additional nuisance regressor for the theta power source analysis investigating the effect of path length differences at different choice points. Including RT as a nuisance regressor specifically for this analysis helped determine whether there were any residual hippocampal theta power effects related to choice point demands during the planning period.

MEG sensor-level analyses

For visualization purposes, scalp power plots were estimated by averaging Morlet wavelet transforms over the entire 3.25s planning period and 4–8Hz frequency window of interest. The sensor-level analysis followed the same EOG variance nuisance regression procedure as source analyses. Subsequently, the linear relationship between trial-by-trial RT and residual 4–8Hz planning period oscillatory power values at each sensor was calculated for every participant.

MEG statistical analyses

There were two main periods of interest, the 1.5s ITI and 3.25s planning phase. For each of the 9 sequential planning regressors of interest (i.e., maze with a small, medium, or large path length at the second and initial points), we constructed parametric regressors based on RT and accuracy (i.e. whether the response was correct). Inferences about these effects were based upon t- and F-tests using the standard summary statistic approach for second level random effects analysis.

A peak voxel significance threshold of $p < 0.05$ FWE corrected for multiple comparisons was used for MEG source analyses. Given the previously hypothesized role of the hippocampus theta rhythm in planning, we report whether peak-voxels in that frequency band and these

regions survive small-volume correction for multiple comparisons ($p < 0.05$) based on a bilateral ROI of the hippocampus (mask created using Neurosynth, Yarkoni, Poldrack, Nichols, Van Essen, & Wager, 2011). All images are displayed at the p < 0.001 uncorrected threshold for illustrative purposes. Additionally, only sources containing a significant peak voxel are displayed.

Post hoc statistical analyses were conducted using 10-mm radius spheres around the respective peak voxel specified in the GLM analysis. This allowed us to compare the effects of different regressors of interest, while ensuring we did not make any biased inferences in our post hoc analyses.

Results

Behavioral performance

Twenty-two participants in the MEG study made correct choices on 87.9 ± 6.13% of sequential planning trials (mean ± SD; non-sequential control trials: 86.4 ± 4.95%), with an average reaction time (RT) of 469 ± 99ms (non-sequential control trials: 363 ± 112ms). Paired t-tests showed that RTs were significantly higher for sequential than non-sequential (i.e. control) trials (t(21) = 9.55; p < .001), without any difference in accuracy (t(21) = 1.42; p = .171). In addition, RTs were strongly inversely correlated with accuracy across MEG participants in both sequential (t(21) = -5.72; p < 0.001) and non-sequential control trials (t(21) = -5.72; p < .001). After accounting for planning demands induced by the path length differences at each choice point (mean path length differences at the two choice points), RTs were still negatively correlated with accuracy in both sequential (t(21) = -5.25; p < .001) and non-sequential control trials (t(21) = -5.14; p < .001). In other words, participants responded faster when they made accurate choices. Moreover, these results demonstrate that RTs directly relate to accurate performance on the spatial planning task.

We then asked whether accuracy and RT were specifically influenced by path length differences and choice point depth, with the aim of disentangling the effects of first/initial versus second/subsequent choice point demands on planning accuracy and RT. Using a repeated measures ANOVA, we looked for an effect of path length difference and choice point depth on accuracy and RTs in MEG participants. We observed a main effect of path length difference on both accuracy (F(2,20) = 9.09; p = .002; Figure 2(a)) and RTs (F(2,20) = 5.06;p = .017; Figure 2(b)), driven by higher accuracy and faster RTs for larger path length differences; as well as a significant interaction between initial (i.e. first) and second (i.e. subsequent) choice points and path length differences on both accuracy (F(4,18) = 11.0;
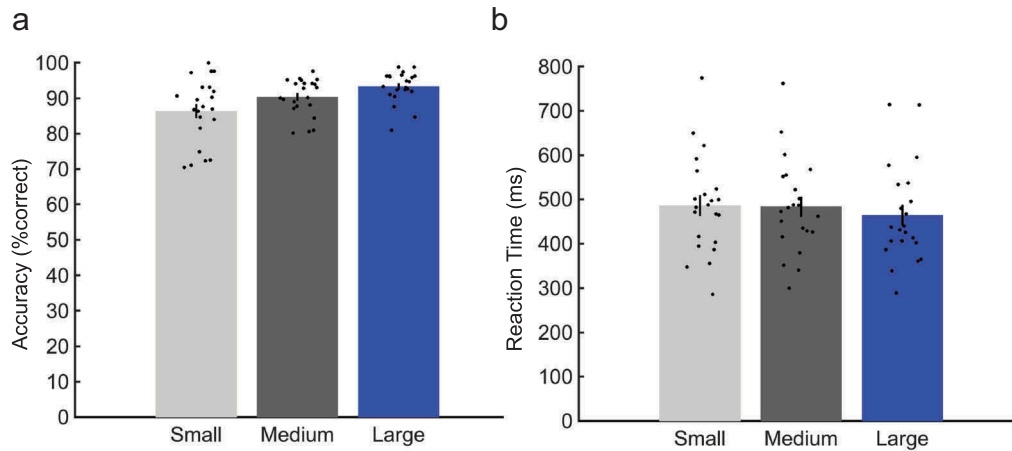
Figure 2. Behavior A. Accuracy. Left: Significant main effect (p = 0.002) of path length differences (small, medium, and large) on choice accuracy, collapsed across initial and second choice points. B. Reaction time. Significant main effect (p = 0.017) of path length differences (small, medium, and large) on reaction times, collapsed across initial and second choice points. All error bars show ± SEM.

p < 0.001) and RTs (F(4,18) = 4.75; p = 0.009). Post-hoc t-tests revealed that this interaction resulted from medium path length differences being significantly less demanding (i.e. producing higher accuracy and faster RTs) when they were at the initial, as opposed to the second, choice point (Accuracy: t(21) = 3.62; p = .002; RT: t(21) = -4.17; p < .001).

MEG analyses

Using MEG source reconstruction, we asked whether 4–8 Hz theta power changes anywhere in the brain were related to differences in spatial planning. As a control to ascertain whether effects were specific to the theta frequency band, we also report power changes in four other canonical frequency bands (delta/low theta: 1–3 Hz, alpha: 9–12Hz, beta: 13–30Hz, and gamma: 30–80Hz). Focusing on RTs, we found a significant negative correlation between 4–8Hz theta power during the sequential planning phase and subsequent RTs in a left hippocampal source (x:-36, y:-20, z:-20, t(21) = -4.28; small volume corrected (SVC) peak-voxel p = .011; Figure 3(a,b)). Specifically, increased hippocampal theta power during planning periods preceded faster decisions – an effect that was also visible at the scalp level (Figure 3(c)). Notably, we did not observe any correlation between theta power and trial-by-trial choice accuracy anywhere in the brain, although this may be due to a relatively small number of errors.

In addition, we found a significant negative correlation between theta power and RTs in the right ventral temporal lobe (x:36, y:-42, z:-26; t(21) = -5.92; family wise error (FWE) corrected peak-voxel p = .012; Fig. S1), which extended into posterior parahippocampal cortex. We did not observe a significant positive correlation between 4–8Hz planning

period theta power and subsequent RTs anywhere in the brain. Elsewhere, we observed 9–12Hz alpha power changes in the right occipital lobe/cerebellum that negatively correlated with RT (x:28, y:-70, z:-22; t(21) = -5.99; FWE corrected peak-voxel p = .014; Fig. S1). However, we observed no other significant correlations between oscillatory power and RT in any other brain regions or frequency band.

To assess whether significant power changes related specifically to sequential planning, we tested whether each correlation described above was stronger for sequential planning trials versus non-sequential/control trials. Using a 10mm sphere around the respective peak voxels, we directly compared sequential versus non-sequential planning correlations with RT and observed that hippocampal RT theta effects selectively corresponded to sequential planning (t(21) = -2.33; p = .03; Figure 3(d)). On the other hand, right ventral temporal/parahippocampal theta (t(21) = -1.38; p = .181; Fig. S1) and occipital/cerebellar alpha effects did not show any significant differences(t(21) = -1.74; p = .095; Fig. S1). We did not observe any significant correlation between alpha or theta power and RT in any brain region during non-sequential control trials.

We then asked whether sequential spatial planning was associated with a general increase in left hippocampal theta power. Again, using a 10mm sphere around the left hippocampal peak, we observed a significant increase in 4–8Hz hippocampal theta power in this region during the sequential planning period versus ITI (t(21) = 3.74; p = .001; Figure 3(e)). Conducting the same sequential planning versus ITI analysis in the other areas exhibiting RT effects, we observed significant increases in both ventral
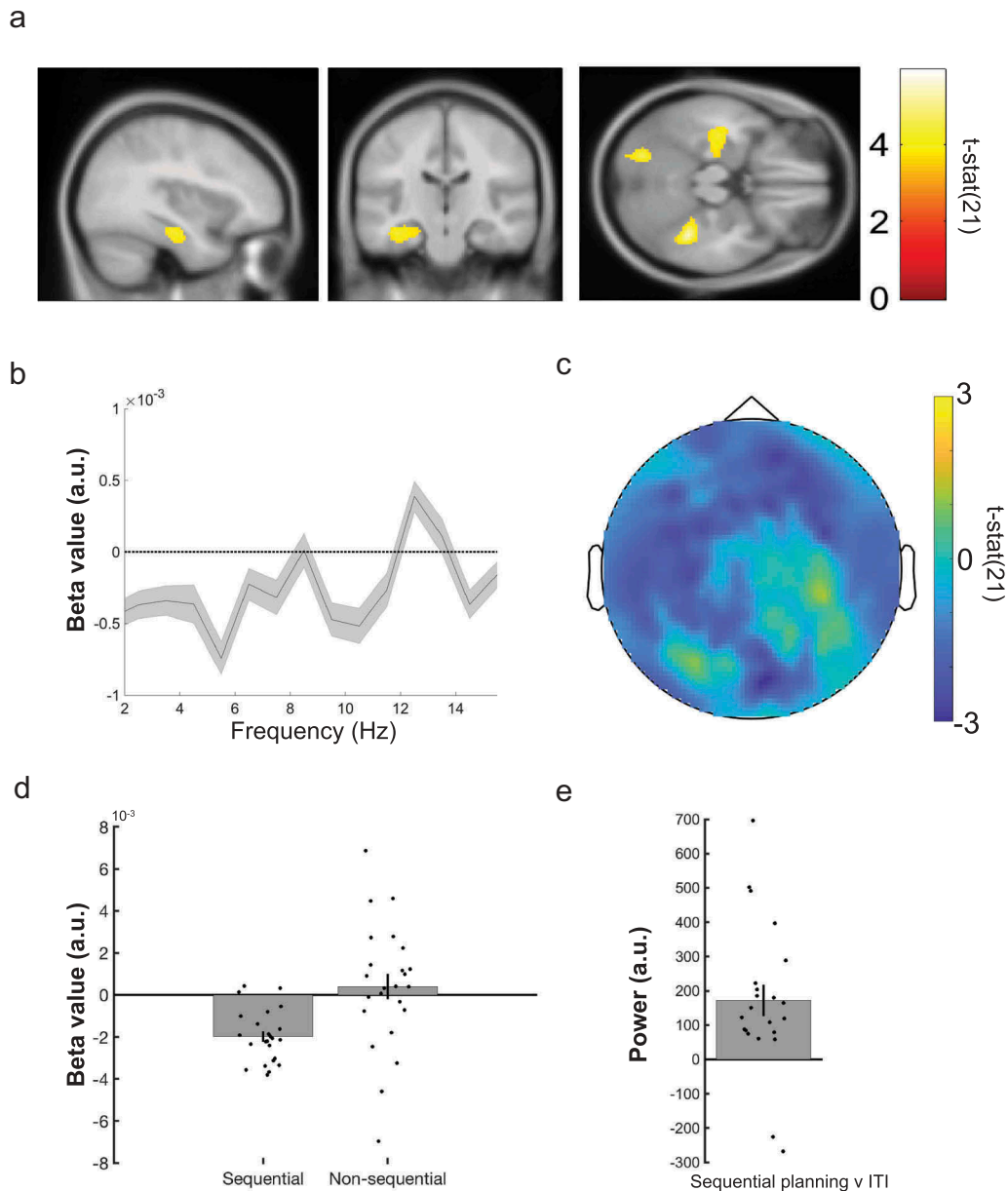
Figure 3. Reaction time correlation with MEG theta power.

A. Linearly Constrained Minimum Variance (LCMV) beamformer source reconstruction image showing significant 4–8 Hz left hippocampal theta power source negative correlation with RT (x:-36, y:-20, z:-20) in 22 healthy participants. Images displayed at the statistical threshold of p < 0.001 uncorrected for visualization purposes. B. Beta value spectrum from 1 to 15 Hz for hippocampal RT theta power effect showing peak negative correlation in the 4–8 Hz theta band. C. Negative 4–8 Hz theta power correlation with RT shown at the scalp level for 22 healthy participants. D. Data from a 10 mm sphere around left hippocampal peak voxel from RT contrast showing a significant difference (t(21) = -2.33; p = .03) between sequential and non-sequential planning trials. E. Data from a 10 mm sphere around left hippocampal peak voxel from RT contrast showing increased theta power (t(21) = 3.74; p = .001) during planning phase versus the ITI period. All error bars show ± SEM.

temporal lobe theta (t(21) = 2.79; p = .011) and occipital alpha (t(21) = 4.44; p < .001) power during sequential planning (Fig. S1).

Finally, isolating hippocampal theta power changes, we tested for the effects of processing demands (path length differences) at initial and second choice points (e.g., quicker RT for mazes with less demanding initial choice points). Using a repeated measures ANOVA (path length difference by choice point depth), we tested whether the left hippocampal region (exhibiting a theta power correlation with RT) also showed an effect of path length differences at initial versus second choice points related to RT. We did not observe any significant effect of path length difference by choice point depth in the left hippocampus (F(4,18) = 1.79; p = .175), or any other brain region.
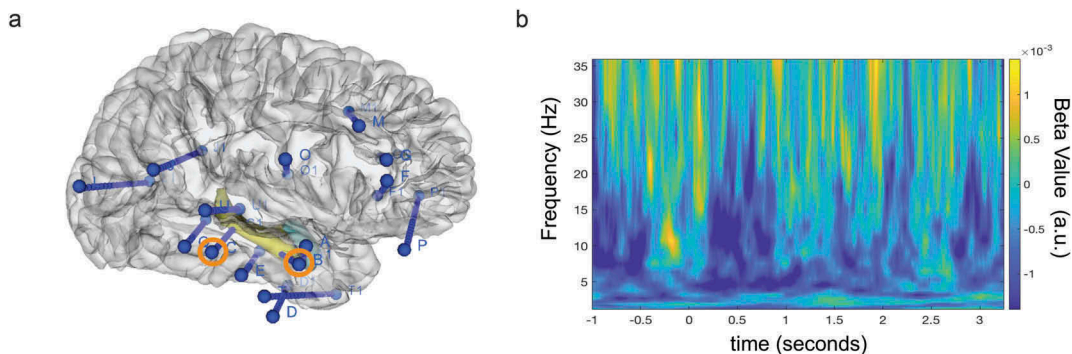
Figure 4. Intracranial EEG data from hippocampal depth electrodes A. Image of electrode locations in the patient overlaid on 3D brain template. Right hippocampal depth electrodes with contacts used in the present analyses are highlighted in orange. B. Time-frequency plot showing a negative correlation over trials between subsequent reaction time (RT) and 4–8 Hz theta power during entire sequential planning period averaged across both hippocampal contacts.

Hippocampal iEEG recordings

Next, to corroborate our source reconstructed MEG effects, we examined changes in low frequency oscillatory power during the 3.25s sequential planning period using intracranial electroencephalography (iEEG) recordings from hippocampal depth electrodes (Figure 4(a)) of a single high performing pre-surgical epilepsy patient (95.5% accuracy; mean RT: 423 ± 123ms). We asked whether iEEG 4–8Hz hippocampal theta power during sequential planning correlated with the patient's subsequent RT. Paralleling the MEG data described above, we observed a negative correlation between ~4–8 Hz hippocampal theta power during the entire 3.25s planning phase and subsequent RT ($r = -0.202$; $p = .035$; Figure 4(b)). This result should be interpreted with caution given the relatively small number of measurements, the presence of an epileptic focus in the same hemisphere, lack of electrode coverage over adequate control regions, and presence of similar correlations at other frequencies. Overall, we observed hippocampal theta (along with alpha and beta) power correlations with RT during the sequential planning period that paralleled the theta effect we observed in the MEG dataset.

General discussion

We examined how the human hippocampal theta rhythm relates to planning sequential decisions in novel environments. Linking hippocampal theta to participants' performance on a spatial planning task, theta power during the planning phase correlated with faster subsequent spatial decisions. Furthermore, decision speed correlated with choice accuracy, regardless of path length differences. Linking the human hippocampal theta rhythm to processing demands, we found that hippocampal theta power selectively corresponded to planning performance in mazes containing multiple choice points during the MEG task.

Our observation of increased hippocampal theta power during spatial decision-making adds to an emerging literature investigating the role of the hippocampal theta rhythm during decision-making in rodents (Johnson & Redish, 2007; Belchior et al., 2014; Pezzulo, Kemere, & van der Meer, 2017; Schmidt et al., 2013; Wikenheiser & Redish, 2015) and humans (Guitart-Masip et al., 2013). Yet, the specific role of the hippocampal theta rhythm in planning has remained unclear; despite recent evidence relating the rodent (Miller et al., 2017) and human hippocampus (Kaplan et al., 2017a) to planning. Additional support for a hippocampal role in planning comes from evidence that hippocampal neurons code the distance to goal locations (Ekstrom et al., 2003; Sarel, Finkelstein, Las, & Ulanovsky, 2017; Villette, Malvache, Tressard, Dupuy, & Cossart, 2015; Watrous, Miller, Qasim, Fried, & Jacobs, 2018). Furthermore, Wikenheiser and Redish (2015) found that firing of place cell sequences coupled to the hippocampal theta rhythm extended further on journeys to distal goal locations. We parallel these findings by showing that hippocampal theta power was selectively related to efficient sequential planning.

Differing from previous MEG/iEEG hippocampal theta studies that observe power increases related generally to enhanced long- or short-term memory performance (Backus, Schoffelen, Szebényi, Hanslmayr, & Doeller, 2016; Guitart-Masip et al., 2013; Lega, Jacobs, & Kahana, 2012; Olsen, Rondina, Riggs, Meltzer, & Ryan, 2013), we find hippocampal theta power effects associated with planning behavior in sequential, but not simpler mazes, during a task requiring little to no learning. Given the known relationship between the hippocampal theta rhythm and spatial trajectories, these findings may relate

to sequential spatial decision-making that focuses on signifying a 'location' update within a sequence of choices. Supporting this explanation, recent work has suggested that the hippocampus can suppress noise in our everyday environment to focus on sub-goals during multi-step planning (Botvinick & Weinstein, 2014) and biophysical models predict that the hippocampal theta rhythm can underlie this type of 'sub-goaling' (Kaplan & Friston, 2018).

Still, several aspects of our results remain unclear. For instance, an alternative explanation for not observing right hemisphere or non-sequential hippocampal theta power spatial planning effects could be that there are multiple theta sources (e.g., anterior right vs posterior left hippocampus) corresponding to sequential and non-sequential RT effects (Miller et al., 2018), which MEG does not have adequate spatial resolution to resolve. Additionally, using eye movements as a nuisance regressor in our MEG data (and not measuring eye movements in our iEEG dataset) prevented us from examining the role of saccadic eye movements in this type of planning, which we have shown in a previous simulation to be a crucial component of our planning task (Kaplan & Friston, 2018). Despite finding hippocampal theta power selectivity to sequential planning, it is important to note that we didn't observe any hypothesized change in theta power related to path length differences at the different choice points. One potential explanation for this null result is that hippocampal distance to goal coding is primarily related to single units, not oscillations (Ekstrom et al., 2003; Sarel et al., 2017; Villette et al., 2015; Watrous et al., 2018). Further evidence supporting this explanation is needed since the direct relationship between behaviorally relevant hippocampal theta power changes and the reactivation of place cell sequences has yet to be characterized during sequential planning. Moving toward this characterization, Watrous et al. (2018) recently observed that human hippocampal single units exhibit phase-locking to the theta rhythm and that this phase-locking encoded information about goal locations during virtual navigation.

We studied multi-step planning in an explicitly spatial domain, but it isn't known whether updating our 'location' to subsequent choice points relates more to the overhead visual searches of the maze or a more abstract decision space (Kaplan, Schuck, & Doeller, 2017b). On one hand, there is mounting evidence of the type I movement-related rodent hippocampal theta rhythm extending to virtual (Bush et al., 2017; Ekstrom et al., 2005, 2003; Kaplan et al., 2012; Watrous, Fried, & Ekstrom, 2011) and real-life navigation in humans (Aghajan et al., 2017; Bohbot, Copara, Gotman, & Ekstrom, 2017). However, evidence from non-spatial domains is lacking. Future work exploring the role of the hippocampal theta rhythm in both perceptual exploration and abstract sequential decisions can determine how generalizable spatial planning-related hippocampal theta effects are to decision-making in other domains.

Data availability statement

The data that support the findings of this study are available on request from the corresponding author, RK. The data are not publicly available due to their containing information that could compromise the privacy of research participants.

Disclosure statement

No potential conflict of interest was reported by the authors.

ORCID

Raphael Kaplan http://orcid.org/0000-0002-5023-1566
Karl J. Friston http://orcid.org/0000-0001-7984-8909

References

Aghajan, Z., Schuette, P., Fields, T. A., Tran, M. E., Siddiqui, S. M., Hasulak, N. R., . . . Suthana, N. (2017). Theta oscillations in the human medial temporal lobe during real-world ambulatory movement. *Current Biology : CB*, *27*, 3743–3751.

Backus, A. R., Schoffelen, J. M., Szebényi, S., Hanslmayr, S., & Doeller, C. F. (2016). Hippocampal-prefrontal theta oscillations support memory integration. *Current Biology : CB*, *26*, 450–457.

Barnes, G. R., & Hillebrand, A. (2003). Statistical flattening of MEG beamformer images. *Human Brain Mapping*, *18*, 1–12.

Belchior, H., Lopes-Dos-Santos, V., Tort, A. B., & Ribeiro, S. (2014). Increase in hippocampal theta oscillations during spatial decision making. *Hippocampus*, *24*, 693–702.

Bohbot, V. D., Copara, M. S., Gotman, J., & Ekstrom, A. D. (2017). Low-frequency theta oscillations in the human hippocampus during real-world and virtual navigation. *Nature Communications*, *8*, 14415.

Botvinick, M., & Weinstein, A. (2014). Model-based hierarchical reinforcement learning and human action control. *Transactions of the Royal Society B: Biological Sciences*, *369* (1655), 20130480

Bush, D., Bisby, J. A., Bird, C. M., Gollwitzer, S., Rodionov, R., Diehl, B., … Burgess, N. (2017). Human hippocampal theta power indicates movement onset and distance travelled. *Proceedings of the National Academy of Sciences of the United States of America*, 114, 12297–12302.

Ekstrom, A. D., Caplan, J. B., Ho, E., Shattuck, K., Fried, I., & Kahana, M. J. (2005). Human hippocampal theta activity during virtual navigation. *Hippocampus*, 15, 881–9.

Ekstrom, A. D., Kahana, M. J., Caplan, J. B., Fields, T. A., Isham, E. A., Newman, E. L., & Fried, I. (2003). Cellular networks underlying human spatial navigation. *Nature*, 425, 184–188.

Fedorov, A., Beichel, R., Kalpathy-Cramer, J., Finet, J., Fillon-Robin, J.-C., Pujol, S., … Kikinis, R. (2012). 3D slicer as an image computing platform for the quantitative imaging network. *Magnetic Resonance Imaging*, 30, 1323–1341.

Guitart-Masip, M., Barnes, G. R., Horner, A., Bauer, M., Dolan, R. J., & Duzel, E. (2013). Synchronization of medial temporal lobe and prefrontal rhythms in human decision making. *The Journal of Neuroscience : the Official Journal of the Society for Neuroscience*, 33, :442–51.

Johnson, A., & Redish, A. D. (2007). Neural ensembles in CA3 transiently encode paths forward of the animal at a decision point. *The Journal of Neuroscience : the Official Journal of the Society for Neuroscience*, 27, 12176–12189.

Kaplan, R., Bush, D., Bisby, J. A., Horner, A. J., Meyer, S. S., & Burgess, N. (2017c). Medial prefrontal-medial temporal theta phase coupling in dynamic spatial imagery. *Journal of Cognitive Neuroscience*, 29, 507–519.

Kaplan, R., Bush, D., Bonnefond, M., Bandettini, P. A., Barnes, G. R., Doeller, C. F., & Burgess, N. (2014). Medial prefrontal theta phase coupling during spatial memory retrieval. *Hippocampus*, 24, 656–665.

Kaplan, R., CF, D., GR, B., Litvak, V., Düzel, E., PA, B., & Burgess, N. (2012). Movement-related theta rhythm in humans: Coordinating self-directed hippocampal learning. *PLoS Biology*, 10, e1001267.

Kaplan, R., & Friston, K. J. (2018). Planning and navigation as active inference. *Biological Cybernetics*, 112, 323–343.

Kaplan, R., King, J., Koster, R., Penny, W. D., Burgess, N., & Friston, K. J. (2017a). The neural representation of prospective choice during spatial planning and decisions. *PLoS Biology*, 15, e1002588.

Kaplan, R., Schuck, N. W., & Doeller, C. F. (2017b). The role of mental maps in decision-making. *Trends in Neurosciences*, 40, 256–259.

Lega, B. C., Jacobs, J., & Kahana, M. J. (2012). Human hippocampal theta oscillations and the formation of episodic memories. *Hippocampus*, 22, :748–61.

Litvak, V., Mattout, J., Kiebel, S., Phillips, C., Henson, R., Kilner, J., … Friston, K. (2011). EEG and MEG data analysis in SPM8. *Computational Intelligence and Neuroscience*, (2011), 852961.

Miller, J., Watrous, A. J., Tsitsiklis, M., Lee, S. A., Sheth, S. A., Schevon, C. A., … Jacobs, J. (2018). Lateralized hippocampal oscillations underlie distinct aspects of human spatial memory and navigation. *Nature Communications*, 9, 2423.

Miller, K. J., Botvinick, M. M., & Brody, C. D. (2017). Dorsal hippocampus contributes to model-planning. *Nature Neuroscience*, 20, 1269–1276.

Nolte, G. (2003). The magnetic lead field theorem in the quasi-static approximation and its use for magnetoencephalography forward calculation in realistic volume conductor. *Physics in Medicine and Biology*, 48, 3637–3652.

O'Keefe, J., & Recce, M. L. (1993). Phase relationship between hippocampal place units and the EEG theta rhythm. *Hippocampus*, 3, 317–330.

Olsen, R. K., Rondina, I. R., Riggs, L., Meltzer, J. A., & Ryan, J. D. (2013). Hippocampal and neocortical oscillatory contributions to visuospatial binding and comparison. *Journal of Experimental Psychology: General*, 142, :1335–45.

Oostenveld, R., Fries, P., Maris, E., & Schoffelen, J. M. (2011). FieldTrip: Open source software for advanced analysis of MEG, EEG, and invasive electrophysiology data. *Computational Intelligence and Neuroscience*, (2011), 156869.

Pezzulo, G., Kemere, C., & van der Meer, M. A. A. (2017). Internally generated hippocampal sequences as a vantage point to probe future-oriented cognition. *Annals of the New York Academy of Sciences*, 1396, 144–165.

Sarel, A., Finkelstein, A., Las, L., & Ulanovsky, N. (2017). Vectorial representation of spatial goals in the hippocampus of bats. *Science*, 355, 176–180.

Schmidt, B., Hinman, J. R., Jacobson, T. K., Szkudlarek, E., Argraves, M., Escabi, M. A., & Markus, E. J. (2013). Dissociation between dorsal and ventral hippocampal theta oscillations during decision-making. *The Journal of Neuroscience : the Official Journal of the Society for Neuroscience*, 33, :6212–24.

Vanderwolf, C. H. (1969). Hippocampal electrical activity and voluntary movement in the rat. *Electroencephalography and Clinical Neurophysiology*, 26, :407–18.

Vila-Vidal, M., Pérez Enriquez, C., Principe, A., Rocamora, R., Deco, G., & Tauste Campo, A. (2019). Low entropy map of brain oscillatory activity identifies spatially localized events: A new method for automated epilepsy focus prediction. *bioRxiv*, 707497.

Villette, V., Malvache, A., Tressard, T., Dupuy, N., & Cossart, R. (2015). Internally recurring hippocampal sequences as a population template of spatiotemporal information. *Neuron*, 88, 357–366.

Watrous, A. J., Fried, I., & Ekstrom, A. D. (2011). Behavioral correlates of human hippocampal delta and theta oscillations during navigation. *Journal of Neurophysiology*, 105, 1747–1755.

Watrous, A. J., Miller, J., Qasim, S. E., Fried, I., & Jacobs, J. (2018). Phase-tuned neuronal firing encodes human contextual representations for navigational goals. *Elife* 7, e32554.

Wikenheiser, A. M., & Redish, A. D. (2015). Hippocampal theta sequences reflects current goals. *Nature Neuroscience*, 18, 289–294.

Yarkoni, T., Poldrack, R. A., Nichols, T. E., Van Essen, D. C., & Wager, T. D. (2011). Large-scale automated synthesis of human functional neuroimaging data. *Nature Methods*, 8, 665–670.